Spin bags and quasiparticles in doped La_2CuO_4

J. B. Grant and A. K. McMahan
Lawrence Livermore National Laboratory, University of California, Livermore, California 94550
(Received 17 March 1992)

Limited configuration-interaction calculations beyond Hartree-Fock are reported for an *ab initio* derived eight-band effective Hamiltonian for La_2CuO_4. These results clearly implicate two important types of configurations, as well as the role of apical-O p_z states, in the nature and dispersion of quasiparticle states associated with one hole doped into the parent insulator. The two types of configurations are spatially inhomogeneous "spin bags" centered about a flipped spin relative to the host antiferromagnetic order, and "doped Néel" configurations that leave the host spin order intact. Taken together these complementary parts are suggestive of the local singlet of Zhang and Rice. It is, however, the latter doped Néel configurations that carry those apical-O p_z components that are primarily responsible for very shallow quasiparticle dispersion from $\mathbf{k}=(\pi/2,\pi/2)$, where the first holes are doped, towards $(\pi,0)$.

I. INTRODUCTION

Realistic calculation of the electronic structure and quasiparticle states in high-temperature superconductors has been complicated by two conflicting challenges. On the one hand, the cuprate materials exhibit effects of strong electron-electron correlation which apparently disallow quantitative one-electron methods such as Hartree-Fock or local-density-functional theory. One signature of these correlation effects, it has been assumed, is the doping-induced transfer of spectral weight into the insulating gaps of parent cuprates like La_2CuO_4. This behavior is observed both in spectroscopic measurements,[1,2] as well as in exact solutions for finite Hubbard clusters.[3-5] On the other hand, the concern for chemical realism points to the need for multiband models of the cuprate electronic structure, which greatly exacerbates attempts at rigorous many-body solutions of large, bulk-like systems. This concern has focused primarily on the relative suitability of one- versus three-band (Cu $d_{x^2-y^2}$ and the two O p_σ orbitals) models.[6-9] However, small but non-negligible occupations of additional states (Cu $d_{3z^2-r^2}$ and apical-O p_z) have also been observed spectroscopically,[10-12] or are implicated theoretically in observable properties of the cuprates,[13-16] suggesting at least a six-band model.

It is the purpose of the present paper to report calculations of the quasiparticle dispersion for one hole doped into insulating La_2CuO_4, which confront both the issue of the correlated nature of the quasiparticle states and that of chemical realism. Specifically, we report limited configuration-interaction (CI) calculations beyond Hartree-Fock (HF) for an *ab initio* derived multiband effective Hamiltonian for La_2CuO_4. We use an eight-band Hamiltonian, which augments the above-mentioned six-band model by the two p_π orbitals associated with O sites in the CuO_2 layers, in order to provide the most accurate representation of the quasiparticle states bordering the insulating gap. However, our results single out the apical-O p_z orbitals as the most important components, beyond those in the familiar three-band model, in regard to their impact on the quasiparticle dispersion. The parameters defining the Hamiltonian were generated using constrained-occupation local-density-functional theory.[17-20]

Recent spatially inhomogeneous HF calculations for Hubbard models of the cuprates have found that the lowest total energy for the hole-doped insulator occurs for localized "spin-bag"-like solutions[21] in the case of one-band[22-27] and three-band[28-30] models. In the latter case, these solutions typically have the mostly O p_σ doped hole localized about a Cu site with a reversed $d_{x^2-y^2}$ spin density relative to the Néel-like background. Similar behavior is observed in Hubbard-modified local-density-functional (LDA+U) calculations.[16] Moreover, these spin-bag solutions exhibit the kind of doping-induced shift of spectral weight that has been thought to be strictly a correlation effect.[3] For both reasons, such spin-bag configurations would appear to be important ingredients in a CI calculation for the cuprates. There are also HF solutions for the hole-doped insulator which are nearby in total energy, yet preserve the Néel-like order of the HF approximation to the insulating parent, and have well-characterized total crystal momentum $\mathbf{k}$. We find that such a "doped Néel" configuration becomes the lowest-energy HF solution for one doped hole *when* apical-O p_z states are included in the Hamiltonian. We argue here that these configurations are also important CI ingredients for the cuprates.

We suggest in this paper that a combination of both spin-bag and doped Néel configurations, each of which may be easily generated by self-consistent HF calculations, is sufficient to account for the quasiparticle dispersion of one hole added to insulating La_2CuO_4. In particular, if $\Psi^n_{\mathbf{k}}$ is the multiconfigurational[31] wave function corresponding to the lowest-energy n-hole state of total momentum $\mathbf{k}$, then

$$\Psi^{N+1}_{\mathbf{k}} \sim A_{\mathbf{k}} \sqrt{\frac{2}{N}} \sum_{\mathbf{R}} e^{i\mathbf{k}\cdot\mathbf{R}} |SB,\mathbf{R}\rangle + B_{\mathbf{k}} |DN,\mathbf{k}\rangle, \qquad (1)$$

where $\mathbf{R}$ ranges over Cu sites on one sublattice of the Néel-ordered HF approximation to the insulating N-hole parent. Here, the spin-bag configuration $|SB,\mathbf{R}\rangle$ is a single, $(N+1)$-hole Slater determinant centered about the flipped Cu spin at $\mathbf{R}$, while the doped Néel configuration $|DN,\mathbf{k}\rangle$ is a linearly independent $(N+1)$-hole determinant which preserves the Néel order and translational symmetry of the parent. We demonstrate numerically that the linear combination in Eq. (1) is primarily responsible for the quasiparticle dispersion of one hole doped into La_2CuO_4, with additional configuration interaction serving mainly to relax the rigid Néel-like order of the HF approximation to the background spin system.

Our results for the quasiparticle dispersion in La_2CuO_4 are essentially the same as those reported in preliminary versions of this work.[13,14] In particular, we suggest that the first holes doped into this insulator occur at wave vector $(\pi/2,\pi/2)$ and are of predominantly O p_σ character. Moving away from $\mathbf{k}=(\pi/2,\pi/2)$ towards $(\pi,0)$, however, we find very shallow dispersion due in large part to a growing admixture of apical-O p_z states, which enter primarily through the doped Néel components of the correlated wave function. Nevertheless, even at $\mathbf{k}=(\pi,0)$ the correlated wave function Eq. (1), as well as one including more extensive configuration interaction, indicates only about ~30% of the doped hole is of apical-O p_z character.

In this paper, we present specific identification of the spin-bag and doped Néel configurations as the "active ingredients" in our earlier configuration-interaction calculations of the quasiparticle dispersion in La_2CuO_4.[13,14] Since the spin-bag configuration has been called[16,30] the mean-field analogue of the Zhang-Rice[32] singlet, we note that the present doped Néel configurations are likely candidates to provide the missing, spin-flipped part of such local singlets, $(|\uparrow\downarrow\rangle+|\downarrow\uparrow\rangle)/\sqrt{2}$. Moreover, the present doped Néel configurations are especially important at $\mathbf{k}=(\pi,0)$, where we find doped holes to have the largest apical-O p_z admixture, and therefore may have an impact on calculations of "anti-Jahn-Teller" polarons.[16]

In the remainder of this paper, we first present our eight-band Hubbard Hamiltonian for La_2CuO_4 in Sec. II. Both periodic and spatially inhomogeneous HF solutions of this effective Hamiltonian are discussed in Sec. III. Various HF-generated configurations are then used as the basis for a systematic limited configuration-interaction treatment in Sec. IV. These calculations are performed both for the eight-band Hamiltonian and for the one-band Hubbard model, where comparison may be made to known exact results in order to test our procedure. Finally, our conclusions are presented in Sec. V, and a short summary in Sec. VI.

II. EFFECTIVE HAMILTONIAN

This section introduces the effective Hamiltonian for La_2CuO_4 that is to be approximately solved in this paper. There is by now ample evidence that local-density-functional theory, in spite of its deficiencies, can provide reasonable values for parameters defining such Hamiltonians.[17–20] The particular approach used here has already been described in detail elsewhere.[20]

A. Choice of states

The states to be included in the effective Hamiltonian are dictated by our goal of providing a realistic description of the insulating gap in La_2CuO_4, and of the dispersion of the quasiparticle states bounding this gap. To motivate our choice, and to establish conventions to be used later in reporting our Hartree-Fock calculations, Fig. 1 shows paramagnetic local-density-functional bands for La_2CuO_4, as obtained by the linear muffin-tin orbitals (LMTO) method and reported elsewhere.[17] These are standard results presented in a nonstandard format: $-\epsilon$ is plotted to give *hole* energies, the predominantly La bands which should occur at the bottom of the figure are omitted for clarity, and the band structure has been folded into the reduced Brillouin zone that would be appropriate to the antiferromagnetic doubled cell. Furthermore, since our effective Hamiltonian will be used to describe a single two-dimensional CuO_2 layer (with associated apical oxygens above and below), we have labeled the irreducible representations in Fig. 1 according to the primitive tetragonal space group $P4/mmm$, using the conventions of Miller and Love.[33] While these $\mathbf{k}$-point *labels* refer to the antiferromagnetic, doubled cell, we follow customary practice for the cuprates in specifying the *coordinates* of the $\mathbf{k}$ vectors relative to the $\mathbf{a}$ and $\mathbf{b}$ axes of the paramagnetic, single unit cell (lattice constant a). Thus $\mathbf{k}_X=(\pi/2,\pi/2)$ and $\mathbf{k}_M=(\pi,0)$ in units of $1/a$, where throughout this paper, $k_z=0$.

The zero of energy in Fig. 1 is the Fermi level, so that these bands incorrectly describe La_2CuO_4 as a metal. It is clear that the insulating gap must open by splitting the doubly degenerate branch near $\epsilon\sim 0$ between $\mathbf{k}_X$ and $\mathbf{k}_M$. The one intrinsic hole per formula unit in insulating La_2CuO_4 would then occupy the full band Γ_4^+–X_2^+–M_4^+–Γ_4^+, and one might anticipate the first doped hole to populate the state X_3^-, or possibly M_1^+. We have examined the paramagnetic LMTO state density along this degenerate X–M branch, and beyond the dominant

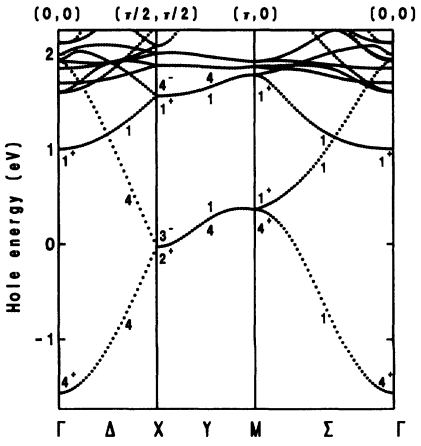

FIG. 1. Paramagnetic local-density-functional hole bands for La_2CuO_4 plotted in the Brillouin zone of the magnetic doubled cell. The zero of energy is the Fermi level.

Cu $d_{x^2-y^2}$ and O p_σ components, find significant ($\sim 9\%$ each) admixtures of both Cu $d_{3z^2-r^2}$ and apical-O p_z components at the M point. There is also a small ($\sim 3\%$) p_π admixture at the X point. To be on the safe side, we have therefore chosen to include all of these components in our effective Hamiltonian. Given two planar and two apical oxygen sites per formula unit, we therefore include a total of eight orbitals ($d_{x^2-y^2}$, $d_{3z^2-r^2}$, $2\times p_\sigma$, $2\times p_\pi$, and $2\times a_z$) per formula unit, leading to an eight-band Hubbard Hamiltonian. Here, and henceforth, we shall designate $2p$ states associated with O atoms in the CuO_2 planes by p (p_σ and p_π) and those associated with the apical-O atoms by a (a_z).

B. Hamiltonian

Table I gives the parameter values defining the eight-band Hubbard Hamiltonian for La_2CuO_4 to be solved in this paper. The parameters were calculated as described in detail elsewhere.[20] In brief, after transforming the local-density-functional one-electron Hamiltonian to a basis of orthogonal Wannier functions, the off-diagonal matrix elements of the transformed Hamiltonian are identified with the hopping matrix elements t of the Hubbard Hamiltonian. By setting these same off-diagonal matrix elements to zero, one may then carry out self-consistent, constrained-occupation calculations, and use the resultant local-density-functional total energy as a function of the occupations to extract the state energies ϵ and monopole contributions to the Coulomb operators U. Higher multipole contributions needed to characterize the full Coulomb operator, and in particular to provide the exchange interactions K, are obtained from spectroscopic data.[20]

TABLE I. Hole state energies ϵ, hopping parameter magnitudes t, Coulomb repulsions U, and exchange interactions K (all in eV) defining the eight-band Hubbard Hamiltonian Eq. (2) for La_2CuO_4. The letters d, p, and a designate Cu($3d$), planar O($2p$), and apical-O($2p$) states, respectively. A single index is used for the singlet ($S=0$) repulsion U between two holes in the same state, while combinations of $\overline{U}\equiv\frac{1}{2}(U^{S=0}+U^{S=1})$ and K give the interactions between two holes in different states on the same site. Intersite $U(p,d)$ and $U(a,d)$ are used regardless of the particular p or d state. The superscript in $t^{(2)}$ indicates second-neighbor interaction.

$\epsilon(d_{x^2-y^2})$	0	$U(d_{x^2-y^2})=U(d_{3z^2-r^2})$	8.96
$\epsilon(d_{3z^2-r^2})$	0.64	$\overline{U}(d_{x^2-y^2},d_{3z^2-r^2})$	6.58
$\epsilon(p_\sigma)$	3.51	$K(d_{x^2-y^2},d_{3z^2-r^2})$	1.19
$\epsilon(p_\pi)$	2.30	$U(p_\sigma)=U(p_\pi)$	4.19
$\epsilon(a_z)$	2.05	$\overline{U}(p_\sigma,p_\pi)$	2.54
$t(d_{x^2-y^2},p_\sigma)$	1.47	$K(p_\sigma,p_\pi)$	0.83
$t(d_{3z^2-r^2},p_\sigma)$	0.50	$U(a_z)$	3.67
$t(d_{3z^2-r^2},a_z)$	0.82	$U(p,d)$	0.52
$t(p_\sigma,p_\sigma)$	0.61	$U(a,d)$	0.18
$t(p_\sigma,p_\pi)$	0.39		
$t(p_\sigma,a_z)$	0.33		
$t(p_\pi,p_\pi)$	0.29		
$t^{(2)}(p_\sigma,p_\sigma)$	0.05		
$t^{(2)}(p_\pi,p_\pi)$	0.02		

The Hamiltonian defined by Table I is

$$H=\sum_{i\alpha\sigma}\epsilon(i\alpha)c^\dagger_{i\alpha\sigma}c_{i\alpha\sigma}+\sum_{i\alpha,j\beta,\sigma}^{i\neq j}t(i\alpha,j\beta)c^\dagger_{i\alpha\sigma}c_{j\beta\sigma}+\sum_{i\alpha}U(i\alpha)n_{i\alpha\uparrow}n_{i\alpha\downarrow}+\frac{1}{2}\sum_{i,\alpha,\beta}^{\alpha\neq\beta}\overline{U}(i\alpha,i\beta)n_{i\alpha}n_{i\beta}$$
$$+\frac{1}{2}\sum_{i,\alpha,\beta}^{\alpha\neq\beta}K(i\alpha,i\beta)\sum_{\sigma,\tau}[c^\dagger_{i\alpha\sigma}c^\dagger_{i\beta\tau}c_{i\alpha\tau}c_{i\beta\sigma}+c^\dagger_{i\alpha\sigma}c^\dagger_{i\alpha\tau}c_{i\beta\tau}c_{i\beta\sigma}]+\frac{1}{2}\sum_{i\alpha,j\beta}^{i\neq j}U(i,j)n_{i\alpha}n_{j\beta}. \quad (2)$$

Here, $c^\dagger_{i\alpha\sigma}$ creates a hole at lattice site i, in Wannier function α, and of spin σ. Also, $n_{i\alpha\sigma}\equiv c^\dagger_{i\alpha\sigma}c_{i\alpha\sigma}$ and $n_{i\alpha}\equiv n_{i\alpha\uparrow}+n_{i\alpha\downarrow}$. Note that i and j each range over the full lattice of both Cu and O sites, so that α and β take on two values ($d_{x^2-y^2}$ and $d_{3z^2-r^2}$) for Cu sites, two values (p_σ and p_π) for planar O sites, and a single value (a_z) for apical-O sites. It is assumed that the matrices $t(i\alpha,j\beta)$, $\overline{U}(i\alpha,i\beta)$, $K(i\alpha,i\beta)$, and $U(i,j)$ are symmetric.

Table I gives the five unique state energies $\epsilon(i\alpha)$, and *magnitudes* of the near-neighbor d-p, p-p, and p-a hopping parameters $t(i\alpha,j\beta)$. More distant t's are assumed to be zero except for the two second-neighbor parameters indicated by $t^{(2)}$. A convenient sign convention is to consider the positive lobes of the $d_{x^2-y^2}$, $d_{3z^2-r^2}$, p_x, p_y, and a_z electron orbitals to lie in the $\pm x$, $\pm z$, $+x$, $+y$, and $+z$ directions, respectively, regardless of position in the unit cell. Then since we are adopting a hole perspective, $t=-|t|$ ($+|t|$) for antibonding (bonding) juxtapositions, e.g., $t(id_{x^2-y^2},jp_\sigma)=-1.47$ eV for $\mathbf{R}_j-\mathbf{R}_i=(a/2,0,0)$ and $+1.47$ eV for $\mathbf{R}_j-\mathbf{R}_i=-(a/2,0,0)$.

The first Coulomb interaction term in Eq. (2) describes the singlet ($S=0$) double occupation of a particular Wannier function $i\alpha$, and the five unique values of $U(i\alpha)\equiv U^{S=0}(i\alpha,i\alpha)$ are given in Table I. The two on-site interaction terms in Eq. (2) involving different functions $\alpha\neq\beta$ pertain to the Cu and planar O sites, where $d_{x^2-y^2}$, $d_{3z^2-r^2}$ and p_σ, p_π pairs of holes are possible, respectively. In each case,

$$U^{S=0}(i\alpha,i\beta)=\overline{U}(i\alpha,i\beta)+K(i\alpha,i\beta), \quad (3)$$

$$U^{S=1}(i\alpha,i\beta)=\overline{U}(i\alpha,i\beta)-K(i\alpha,i\beta). \quad (4)$$

In fact, within the limited manifolds considered here, two numbers $\overline{U}$ and K characterize the full intrasite (Cu or O) Coulomb operator, viz.,

$$U(i\alpha)=U(i\beta)=\overline{U}(i\alpha,i\beta)+2K(i\alpha,i\beta). \quad (5)$$

Finally, we consider only scalar intersite Coulomb repulsions between near-neighbor Cu and O sites, which are assumed independent of the particular states (α and β) occupied on the two sites, as given by the last term in Eq. (2).

There are a number of small differences between the parameters in Table I and those reported in Ref. 20 which should be noted. The summary table presented in that reference included averages over uncertainties related to the choice of atomic-sphere radii in the LMTO method, as well as estimates of supercell convergence. Since these effects were relatively modest, in the present work we take parameter values obtained from a single choice of the atomic-sphere radii and just the doubled supercell. The parameters in Table I of the present work therefore correspond to the case 2 values in Table III of Ref. 20. There is precise correspondence for the Coulomb interactions, noting that $K(d_{x^2-y^2}, d_{3z^2-r^2}) = \frac{4}{49}F^2(3d,3d) + \frac{15}{441}F^4(3d,3d)$ and $K(p_\sigma, p_\pi) = \frac{3}{25}F^2(2p,2p)$ in terms of the Slater integrals of Ref. 20. The hopping parameters are also identical aside from the new values involving the p_π Wannier functions, the second neighbor $t^{(2)}(p_\sigma, p_\sigma)$, and a slightly smaller value of $t(p_\sigma, a_z)$. In regard to the last difference, the hopping parameters in Ref. 20 were determined by equating LMTO matrices to near-neighbor tight-binding expressions at $\mathbf{k} = (\pi,\pi)$. Extracting the parameters at other $\mathbf{k}$ points generally gives about the same values, although the variations were larger for $t(p_\sigma, a_z)$, and so we used the value obtained at the more important $\mathbf{k}_M = (\pi, 0)$ in that case. Finally, there are small differences in the state energies $\epsilon(i\alpha)$ in Table I. These follow from the fact that we have now used $k_z = 0$ averages, rather than full Brillouin-zone averages, to extract the crystal-field splittings $\Delta\varepsilon_{qlm}$ of Ref. 20, while also accounting for the two second-neighbor hopping parameters in Table I.

III. HARTREE-FOCK

We present here unrestricted or spin-polarized Hartree-Fock (HF) solutions of the eight-band Hamiltonian in Eq. (2). After a brief description of the computational details, we discuss the insulating band structure which such HF calculations yield for the periodic antiferromagnetic lattice. We then consider spatially inhomogeneous HF solutions[22-30] which will play a crucial role in our subsequent limited configuration-interaction calculations.

A. Formalism

We take the HF wave function to be an eigenfunction of the z component, S_z, of the total spin S, as there is no evidence of canting angles away from the quantization axis in HF solutions for one-band[24] or three-band[28] models in the cuprate parameter regime:

$$\Psi_{\rm HF} = \prod_{\kappa\sigma}^{\rm occ} c^\dagger_{\kappa\sigma}|{\rm vac}\rangle. \tag{6}$$

Here, the vacuum $|{\rm vac}\rangle$ contains no holes, while $c^\dagger_{\kappa\sigma}$ creates a hole in the HF orbital labeled κ, spin σ, which is a linear combination [$c_{\kappa\sigma} = \sum_{i\alpha} a_{\kappa\sigma}(i\alpha)c_{i\alpha\sigma}$] of the localized basis orbitals (indexed by $i\alpha\sigma$) in which the eight-band Hamiltonian H is defined. Minimizing the HF total energy

$$E_{\rm HF} \equiv \langle\Psi_{\rm HF}|H|\Psi_{\rm HF}\rangle/\langle\Psi_{\rm HF}|\Psi_{\rm HF}\rangle \tag{7}$$

with respect to the coefficients $a_{\kappa\sigma}(i\alpha)$ yields the corresponding self-consistent HF equation

$$\sum_{j\beta}\left[\epsilon(i\alpha)\delta_{ij}\delta_{\alpha\beta} + t(i\alpha, j\beta) + \tilde{t}_\sigma(i\alpha, j\beta)\right] a_{\kappa\sigma}(j\beta) = \varepsilon_{\kappa\sigma}a_{\kappa\sigma}(i\alpha). \tag{8}$$

The Coulomb parameters enter through $\tilde{t}_\sigma(i\alpha, j\beta)$:

$$\tilde{t}_\sigma(i\alpha,i\alpha) = U(i\alpha)\rho_{-\sigma}(i\alpha,i\alpha) + \sum_\beta^{\beta\neq\alpha}\left[\overline{U}(i\alpha,i\beta)\sum_\tau \rho_\tau(i\beta,i\beta) - K(i\alpha,i\beta)\rho_\sigma(i\beta,i\beta)\right] + \sum_{j\beta}^{j\neq i} U(i,j)\sum_\tau \rho_\tau(j\beta,j\beta), \tag{9}$$

$$\tilde{t}_\sigma(i\alpha,i\beta) = -\overline{U}(i\alpha,i\beta)\rho_\sigma(i\beta,i\alpha) + K(i\alpha,i\beta)\left[\rho_{-\sigma}(i\alpha,i\beta) + \sum_\tau \rho_\tau(i\beta,i\alpha)\right], \tag{10}$$

$$\tilde{t}_\sigma(i\alpha,j\beta) = -U(i,j)\rho_\sigma(j\beta,i\alpha), \tag{11}$$

where $\rho_\sigma(i\alpha, j\beta)$ is the one-particle density matrix defined by

$$\rho_\sigma(i\alpha,j\beta) \equiv \langle\Psi_{\rm HF}|c^\dagger_{i\alpha\sigma}c_{j\beta\sigma}|\Psi_{\rm HF}\rangle = \sum_{\kappa\sigma}^{\rm occ} a_{\kappa\sigma}(i\alpha)a^*_{\kappa\sigma}(j\beta). \tag{12}$$

Here, Eqs. (10) and (11) are restricted to $\alpha\neq\beta$ and $i\neq j$, respectively, $-\sigma$ indicates the spin opposite to σ, and "occ" in Eqs. (6) and (12) refers to a product or sum over the hole-occupied HF orbitals.

The nonlinear system of equations, Eqs. (8)–(12), are solved self-consistently by using the density matrix calculated at one iteration to evaluate $\tilde{t}_\sigma(i\alpha, j\beta)$ for the next

iteration. Because the HF method requires identifying which orbitals are occupied at each iteration, it is easy to select a desired eigenvalue for S_z. Note, however, that $\Psi_{\rm HF}$ is not an eigenfunction of the total spin. Expectations of both S_z and S^2 may be obtained from the density matrix

$$\langle\Psi_{\rm HF}|S_z|\Psi_{\rm HF}\rangle = \tfrac{1}{2}\sum_{i\alpha}[\rho_\uparrow(i\alpha,i\alpha)-\rho_\downarrow(i\alpha,i\alpha)]\,, \qquad (13)$$

$$\langle\Psi_{\rm HF}|(S^2-S_z^2-S_z)|\Psi_{\rm HF}\rangle = \sum_{i\alpha,j\beta}\rho_\downarrow(i\alpha,j\beta)\,[\delta_{ij}\delta_{\alpha\beta}-\rho_\uparrow(i\alpha,j\beta)]\,. \qquad (14)$$

It is also straightforward to choose $\Psi_{\rm HF}$ to be a particular eigenfunction of the total momentum, and to reformulate Eq. (8) in reciprocal space. However, later we will be interested in spatially inhomogeneous HF solutions and so will work in direct space throughout this paper, except for generating the HF band structure to be reported in the next subsection.

B. Antiferromagnetic insulator

Figure 2 shows the one-particle eigenvalues $\varepsilon_{\kappa\sigma}=\varepsilon_{\mathbf{k}m\sigma}$ of Eq. (8) for the up-spin case, obtained from a HF solution of the eight-band Hamiltonian for one hole per formula unit. These particular HF calculations were carried out in $\mathbf{k}$ space for the antiferromagnetic doubled cell, and so the compound index κ represents both the appropriate $\mathbf{k}$ vector and band index m. Note that the nondispersive band just above $\varepsilon = 2$ eV is from the non-bonding a_z combination. A clear insulating gap is evident in these results, which may be contrasted with the paramagnetic LMTO band structure in Fig. 1. The intrinsic holes, one per formula unit, occupy the spin-degenerate hole band below the gap (Γ_4^+–X_2^+–M_4^+–Γ_4^+ in Fig. 2 for $\sigma=\uparrow$), and

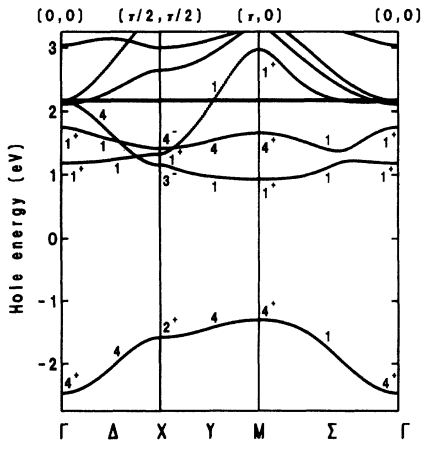

FIG. 2. Hartree-Fock up-spin hole bands for antiferromagnetic La_2CuO_4 obtained from solution of the eight-band effective Hamiltonian defined by Eq. (2), plotted in the Brillouin zone of the doubled cell.

are of predominant Cu($d_{x^2-y^2}$) character (65% $d_{x^2-y^2}$ and 33% p_σ). The lowest levels just above the gap are candidates for holes doped into La_2CuO_4. Of particular interest are the X_3^- state (62% p_σ, 23% $d_{x^2-y^2}$, and 15% p_π) and the M_1^+ state (52% a_z, 25% p_σ, 14% $d_{3z^2-r^2}$, and 8% $d_{x^2-y^2}$). The former, X_3^-, state is the lowest available level for doped holes which is consistent with indications from polarized spectroscopy measurements that the first doped holes have strongly x,y-polarized O($2p$) components.[12,34] However, the latter M_1^+ state is 0.23 eV below the X_3^- state in Fig. 2, and therefore according to these calculations the state which should be occupied by the first doped holes. This discrepancy in level ordering, the counterpart of which has been seen in a number of finite-cluster calculations,[35] was one of the motivations for going beyond spatially homogeneous HF in this work.

On the other hand, the results in Fig. 2 are to a large extent realistic and instructive. There is, for example, an important interplay between spin and symmetry which illuminates the manner in which HF successfully avoids double occupation. Note first that the band structure in Fig. 2 is strictly only for the up-spin states. While $\varepsilon_{\mathbf{k}m\downarrow}=\varepsilon_{\mathbf{k}m\uparrow}$, the symmetry labels along the X–M line become interchanged ($X_2^+\leftrightarrow X_3^-$, $X_1^+\leftrightarrow X_4^-$, $Y_4\leftrightarrow Y_1$, $M_4^+\leftrightarrow M_1^+$) for the opposite spin, signaling sublattice segregation. There is, in fact, complete segregation of $d_{x^2-y^2}\uparrow$ and $d_{x^2-y^2}\downarrow$ components onto different sublattices along the X-M line, as is evident for the end points from the orbital sketches in Fig. 3. While this symmetry-imposed constraint is relaxed elsewhere in the Brillouin zone, the effective segregation persists so that the average minority-spin $d_{x^2-y^2}$ density is only 0.015 holes per Cu site in these HF calculations.

The spin-symmetry interplay is also indicative of local singlet or triplet relationships between intrinsic and doped holes. Consider adding an up-spin hole at X. The resultant X_3^-, mostly-p_σ molecular orbital has b_{1g} (x^2-y^2) symmetry *only* about Cu sites with down spins [shaded plaquettes in Fig. 3(a)]. These HF solutions, therefore, exhibit a natural matching of intrinsic-Cu and doped-O molecular orbitals of b_{1g} symmetry yet *opposite* spin, suggestive of the $^1A_{1g}$ singlet solutions of two-hole CuO_n clusters,[35] as well as of the Zhang-Rice singlet.[32] Now consider points away from X along the X-M line, where b_{1g} and a_{1g} ($3z^2-r^2$) symmetries are permitted to mix. A given molecular orbital for such a $\mathbf{k}$ point will appear locally b_{1g} on one sublattice, and a_{1g} on the other. In particular, the local relationship between an up-spin hole doped at M_1^+ and the intrinsic b_{1g} Cu holes will be $b_{1g}^\uparrow b_{1g}^\downarrow$ or $^1A_{1g}$ on one sublattice [fully shaded plaquette in Fig. 3(c)], and $a_{1g}^\uparrow b_{1g}^\uparrow$ or $^3B_{1g}$ on the other sublattice [central, partially shaded plaquette in Fig. 3(c)]. From the decomposition of the M_1^+ orbital given above, the proportions are 8% $^1A_{1g}$ ($d_{x^2-y^2}$), 66% $^3B_{1g}$ (a_z and $d_{3z^2-r^2}$), and 25% both $^1A_{1g}$ and $^3B_{1g}$ (p_σ), that is, predominantly $^3B_{1g}$. An essential point here is that the X_3^-, M_1^+ level ordering in Fig. 2 is the itinerant counterpart of the $^1A_{1g}$, $^3B_{1g}$ ordering in two-hole solutions for CuO_n clusters.[35]

We have previously noted that HF calculations such

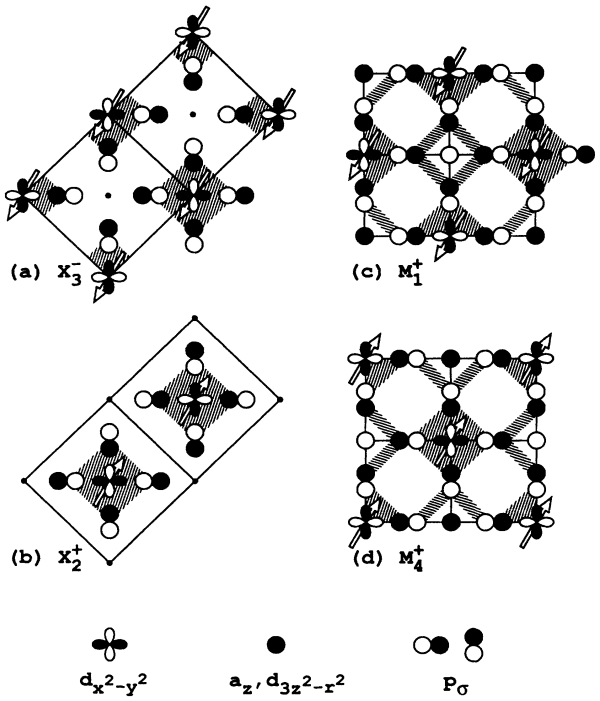

FIG. 3. Sketch of the one-particle orbitals bordering the insulating gap in Fig. 2 at the X and M points. Fully shaded plaquettes indicate local b_{1g} symmetry; partially shaded plaquettes as at the center of (c), local a_{1g} symmetry. Arrows indicate directions of $d_{x^2-y^2}$ spin density in the HF ground state. Apical-O p_z is abbreviated a_z.

as those reported here provide reasonable values for the insulating gap of a variety of magnetic compounds like La_2CuO_4.[13] In the present case, the 2.2-eV M_4^+–M_1^+ separation in Fig. 2 may be compared to experimental gap values in the range 1.8–2.0 eV for La_2CuO_4.[36] However, two cautionary remarks should be made. First, true HF calculations, carried out in first quantization where all parameters are self-consistently generated by the HF calculation itself, may be expected to give insulating gaps characteristic of unscreened Coulomb interactions. Such calculations for closely related $CaCuO_2$, for example, yield a 13.5-eV gap.[37] While HF does not screen two-body interactions, it, or any one-electron approach, is capable of screening an *external* nonuniform potential.[38] Constrained-occupation local-density-functional calculations obtain *screened* Coulomb interactions by effectively treating added charge at a given site in this manner.[17–20] When such screened interactions are built into second-quantized Hamiltonians as here, or added to the one-electron Schrödinger equation as in the "LDA+U" approach,[16,39] one appears to obtain insulating gaps of roughly the right size. Second, our CI calculations to be reported in Sec. IV indicate that correlation corrections to the gap in Fig. 2 are not small. In particular, they drop the X_3^- state slightly below M_1^+ and yield a final predicted 1.5-eV gap from M_4^+ to X_3^- for the effective Hamiltonian given by Eq. (2).

C. The doped insulator

We now consider HF solutions for the case of one hole added to the antiferromagnetic insulator, that is, $n=N+1$ holes where N is the number of formula units. Solutions of one-band[22–27] and three-band[28–30] Hubbard models for $N+1$ holes obtain the lowest energy when there is a spatially inhomogeneous relaxation of the host spin system about the additional hole, resulting in localization of the doped particle, thus forming a spin polaron or spin bag.[21] We also find this to be the case for a three-band model based on the parameters in Table I. However, when we include a_z states in the effective Hamiltonian, we find a lower-energy HF solution which retains the Néel order of the insulating parent. More generally, we find a variety of low-energy, metastable $(N+1)$-hole HF solutions which range in translational symmetry from localized (spin bag) to having the double-cell periodicity of the Néel-ordered parent (doped Néel).

The heritage of the spin-bag and doped Néel limiting cases is already evident in N-hole HF solutions for $M_S=1$ and 0, respectively, where M_S is the eigenvalue of the z component of the total spin. The flipped spin at $\mathbf{R}$ required to achieve $M_S=1$ in the former case breaks translational symmetry, leading to localized or scatteringlike orbitals. By adding a down-spin hole to the lowest available level, one may create an $(N+1)$-hole, $M_S=\frac{1}{2}$ spin-bag configuration $|SB,\mathbf{R}\rangle$. The orbitals in the latter Néel ($M_S=0$) solution, on the other hand, are Bloch functions. By adding an up-spin hole to the lowest available level for a given $\mathbf{k}$, one may create an $(N+1)$-hole, $M_S=\frac{1}{2}$ doped Néel configuration $|DN,\mathbf{k}\rangle$. We use just such configurations obtained by "rigid-band doping" of self-consistent N-hole HF solutions in our CI calculations reported in Sec. IV. Here, we take these configurations as starting points for iteration to $(N+1)$-hole self-consistency. The calculations were carried out for $n=17$ holes in 16-formula-unit clusters with periodic boundary conditions. In spite of the differing ancestry just discussed, our language below will reflect the fact that all $M_S=\frac{1}{2}$, $(N+1)$-hole HF solutions represent a net up-spin addition relative to the N-hole *ground state* which is $M_S=0$.

We begin with the spin-bag solution, for which $E_{\rm HF}^{17}=-31.736$ eV, a decrease of 0.065 eV from the energy of the starting configuration obtained by rigid-band doping. Figure 4(a) presents the combined spin and charge densities for this solution, where opposite edges in the figure are equivalent, reflecting our periodic boundary conditions. The length and direction of the arrows give the $\alpha=d_{x^2-y^2}$ spin density $\langle\Psi_{\rm HF}^{17}|(n_{i\alpha\uparrow}-n_{i\alpha\downarrow})|\Psi_{\rm HF}^{17}\rangle$. The corresponding $\alpha=p_\sigma$ spin density is an order of magnitude smaller, and is not visible. Following Zaanen and Gunnarsson,[28] the radii of the circles gives the *change* in the charge density brought about by adding the 17th hole to the 16-hole Néel solution, i.e., $\langle\Psi_{\rm HF}^{17}|n_{i\alpha}|\Psi_{\rm HF}^{17}\rangle-\langle\Psi_{\rm HF}^{16}|n_{i\alpha}|\Psi_{\rm HF}^{16}\rangle$, where $n_{i\alpha}\equiv n_{i\alpha\uparrow}+n_{i\alpha\downarrow}$. Results are shown for both $\alpha=d_{x^2-y^2}$ and p_σ, although a minimal point size is maintained in the latter case as a reminder of the O positions. About 21% of the added density occurs in non-three-band orbitals, mostly a_z, and

is due to differences in the 16 lowest-energy HF orbitals between $\Psi_{\rm HF}^{17}$ and $\Psi_{\rm HF}^{16}$. It is clear from Fig. 4(a) that the predominantly O p_σ doped hole in the spin-bag configuration $|SB,\mathbf{R}\rangle$ is localized about the flipped Cu spin at $\mathbf{R}$ relative to the original Néel order.[28,30] Actually,

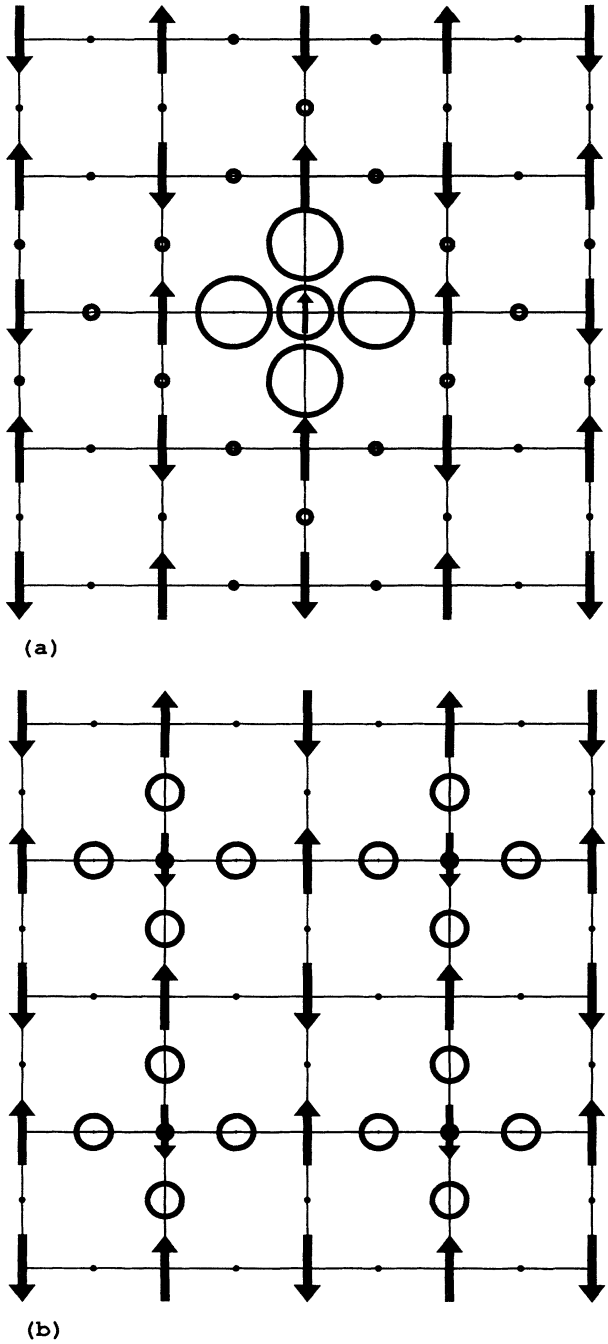

FIG. 4. Self-consistent Hartree-Fock solutions of the eight-band effective Hamiltonian carried out for 17 holes in a periodic 16-formula-unit cluster: (a) localized spin bag, and (b) 2×2 relaxation of the X-point doped Néel configuration. The size and direction of the arrows indicates $d_{x^2-y^2}$ spin density, while the radii of the circles give the added $d_{x^2-y^2}$ and p_σ charge density relative to the Hartree-Fock values for the 16-hole insulator.

the magnitude of the $d_{x^2-y^2}$ spin density at the central Cu is 0.37 in our results, about half the ~0.62 value at Cu sites on the boundaries of the cell.

The spin-bag configuration $|SB,\mathbf{R}\rangle$ illustrated in Fig. 4(a) is not an eigenstate of the total crystal momentum corresponding to the magnetic double cell. However, one may form a Bloch projection which does have well characterized $\mathbf{k}$,

$$|SB,\mathbf{k}\rangle=\sqrt{\frac{2}{N}}\sum_{\mathbf{R}}e^{i\mathbf{k}\cdot\mathbf{R}}|SB,\mathbf{R}\rangle, \tag{15}$$

where $\mathbf{R}$ is confined to Cu sites on the down-spin Néel sublattice. We find that the expectation $\langle SB,\mathbf{k}|H|SB,\mathbf{k}\rangle$ leads to a 1.26-eV bandwidth as a function of $\mathbf{k}$, and that its energy at $\mathbf{k}_X$ is 0.284 eV *below* that of the localized spin-bag $|SB,\mathbf{R}\rangle$. However, we believe that the projection $|SB,\mathbf{k}\rangle$ is intrinsically multiconfigurational,[31] and therefore cannot possibly be a HF solution itself. This fact may be easily proved in the strong-coupling limit of the one-band Hubbard model, where[24]

$$|SB,\mathbf{R}_i\rangle=\left[\frac{1}{\sqrt{2}}c_{i\downarrow}^\dagger+\frac{1}{\sqrt{8}}\left(c_{i_1\downarrow}^\dagger+c_{i_2\downarrow}^\dagger+c_{i_3\downarrow}^\dagger+c_{i_4\downarrow}^\dagger\right)\right]\times c_{i\uparrow}^\dagger c_{i\downarrow}|\text{Néel}\rangle. \tag{16}$$

Here, the sites $\mathbf{R}_i$ in Eq. (16) are restricted to the down-spin sublattice of the Néel configuration, and i_1, i_2, i_3, and i_4 are the four near neighbors of i. The Bloch projection, Eq. (15), of this single Slater determinant leads to nonintegral eigenvalues of the corresponding one-particle density matrix, demonstrating the multiconfigurational nature of $|SB,\mathbf{k}\rangle$ in this case.

Our lowest-energy HF solution ($E_{\rm HF}^{17}=-31.814$ eV) is obtained by iterating from a starting configuration in which an up-spin hole is added to the empty M_1^+ Bloch orbital of the Néel ground state of the insulating parent (see Fig. 2). There is very little relaxation of this doped Néel configuration $|DN,\mathbf{k}_M\rangle$ from the starting point; the translational symmetry persists, and the total energy is lowered by only 0.004 eV. There is a slight reduction (0.01 holes per site) in the minority, down-spin $d_{x^2-y^2}$ density at the majority up-spin Cu sites, essentially a backflow response to the added $d_{3z^2-r^2}$ component of the M_1^+ orbital due to $U(d_{x^2-y^2},d_{3z^2-r^2})$.

If the same procedure is repeated starting with an added hole in the empty X_3^- orbital of the Néel-ordered parent, the self-consistent solution ($E_{\rm HF}^{17}=-31.625$ eV) illustrated in Fig. 4(b) is obtained. Here the self-consistent total energy is 0.045 eV below the starting point, and the translational symmetry has been reduced from the $\sqrt{2}\times\sqrt{2}$ double cell to a 2×2 quadruple cell. The segregation of the added p_σ density onto half of the in-plane O sites is, in part, allowed by the degeneracy of the X point in the Brillouin zone of the double cell, i.e., $\mathbf{k}_X=(\pi/2,\pi/2)$, $(\pi/2,-\pi/2)$. However, there is an additional 19% reduction of $d_{x^2-y^2}$ spin density at the four centers of the added p_σ charge density, an obvious spin-bag-like tendency, which reduces the translational symmetry. We find the solution in Fig. 4(b) to also

be metastable in three-band calculations. By perturbing this solution we have also obtained something like Fig. 4(a) except that the central Cu spin is not reversed, although, only for the eight-band case.

Finally, it should be noted that we find CI calculations including both spin-bag and doped Néel configurations to provide slightly lower total energies when these configurations are generated by rigid-band doping of self-consistent N-hole HF solutions, rather than when generated from fully self-consistent $(N+1)$-hole calculations as here. This approach also avoids $\mathbf{k}$-dependent variations in translational symmetry as found here for the doped Néel configurations at $\mathbf{k}_X$ and $\mathbf{k}_M$. Another point of interest is that doped Néel configurations become redundant in such CI calculations in the limit of truly one-band-like behavior. This is evident in the strong-coupling limit of the one-band Hubbard model, where $|DN,\mathbf{k}\rangle$ is the Bloch projection of the first term, $c^\dagger_{i\uparrow}|\text{Néel}\rangle$, in Eq. (16). Since the coefficients ($1/\sqrt{2}$ and $1/\sqrt{8}$) in Eq. (16) have already been optimized by the mean-field solution for $|SB,\mathbf{R}\rangle$,[24] doped Néel configurations are irrelevant for this limit of the one-band model. In effect, the importance of $|DN,\mathbf{k}\rangle$ is a measure of the different character (e.g., composition) of the doped versus intrinsic holes.

D. Doping-induced changes in state density

The doping-induced changes in state density, which are exhibited by spatially inhomogeneous HF solutions of Hubbard models for the cuprates,[22–30] have important repercussions for the level-ordering discrepancy discussed in Sec. III B. To illustrate this point, Fig. 5 compares the one-hole density of states obtained from self-consistent HF solutions of our eight-band Hamiltonian for (a) $n=N+1$ holes (localized spin-bag solution), (b) $n=N$ holes (Néel-ordered insulator of Fig. 2), and (c) $n=N-1$ holes (also a spin-bag solution). The calculations were carried out for a periodic 16-formula-unit ($N=16$) cluster, and so the resultant discrete states have been broadened by Gaussians of 0.5-eV full width at half maximum. The solid lines represent the total state density, the hatched area, the O($2p$) contribution, and the open area in between the two, the Cu($3d$) contribution. Note that the mostly Cu($3d$) "upper Hubbard band" of the electron representation lies to the left, between about -3 and -1 eV in the hole perspective of Fig. 5. For convenience we will refer to this band and the predominantly O($2p$) band at higher hole energies as simply the Cu and O bands, respectively.

Two interesting changes in the HF state density occur when an $(N+1)$st hole is added to the N-hole insulator in Fig. 5(b). First, one of the N states from the Cu band is transferred upward to $\varepsilon\sim 0$ eV, as indicated by the arrow labeled "$\sim d_{x^2-y^2}$" in Fig. 5(a). This is the kind of anomalous transfer of spectral weight discussed by Eskes *et al.*,[3] which is therefore not exclusively a correlation effect, but may be approximately reproduced in one-particle theory when the solution includes localized orbitals. Second, the first O band state above the Fermi level ε_F in Fig. 5(b) is mostly a_z in character, whereas the O band state *actually* occupied by the $(N+1)$st hole is mostly p_σ as indicated by the arrow labeled "$\sim p_\sigma$" in Fig. 5(a).

While the latter behavior is related to the resolution of the level-ordering discrepancy discussed in Sec. III B, our CI calculations in the next section will show this resolution to be more complex. In particular, the correlated $(N+1)$-hole wave function $\Psi^{N+1}_{\mathbf{k}}$ is a $\mathbf{k}$-dependent mixture of the (Bloch-projected) spin bag in Fig. 5(a) and the doped Néel counterpart of Fig. 5(b). Nevertheless, our numerical results do suggest that the spin bag is the more important component at $\mathbf{k}_X=(\pi/2,\pi/2)$, where the first holes are doped, and that at this $\mathbf{k}$ point there are *no* a_{1g} (a_z or $d_{3z^2-r^2}$) contributions to the doped hole arising from the doped Néel components in $\Psi^{N+1}_{\mathbf{k}}$. The leading $\sim a_z$ edge of the O band in Fig. 5(b), it should be noted, arises from states at $\mathbf{k}_M=(\pi,0)$.

Given the caveats just mentioned, it is of interest to examine the compositional dependence of the prepeak just below ε_F in Fig. 5(a), which may be compared with polarized spectroscopy experiments.[12,34] Such measurements will sample *both* the Cu- and O-rich states labeled in Fig. 5(a), whose $d_{x^2-y^2}$, p_σ proportions are 58%, 33% and 31%, 56%, respectively. The net decomposition of

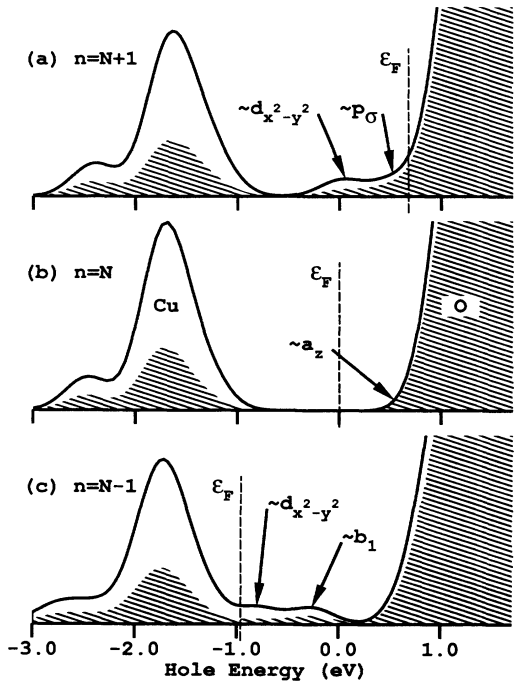

FIG. 5. Broadened one-hole density of states for n-hole Hartree-Fock solutions of the eight-band effective Hamiltonian carried out for 16-formula-unit periodic clusters: (a) $n=17$ localized spin bag, (b) $n=16$ Néel-ordered insulator, and (c) $n=15$ localized spin bag. The Fermi levels ε_F are shown, while the arrows labeled $\sim d_{x^2-y^2}$, $\sim p_\sigma$, $\sim a_z$, and $\sim b_1$ denote the dominant composition at the energies indicated. Here, a_z means apical-O p_z, and b_1, comparable $d_{x^2-y^2}$ and p_σ components.

both HF one-particle orbitals taken together is 44.6% $d_{x^2-y^2}$, 44.5% p_σ, 6.8% a_z, 2.1% $d_{3z^2-r^2}$, and 2.0% p_π. These numbers lead to a 14.6% ratio of O($2p$) components which are polarized in the z direction relative to those polarized in the x,y plane, at a doping level $x = \frac{1}{16} = 0.0625$, comparable to the measured 13±1% value obtained at $x = 0.07$ by Chen and co-workers.[12]

Finally, since we do not evaluate the spectral function in our subsequent more rigorous CI calculations, we would like to note here that a similar decomposition is provided by the charges $Q^n_\alpha \equiv \sum_{i\sigma}\langle\Psi^n|c^\dagger_{i\alpha\sigma}c_{i\alpha\sigma}|\Psi^n\rangle$, where Ψ^n in the present case is one of the n-hole HF wave functions corresponding to Fig. 5. If we consider the composition of an intrinsic Cu-rich hole to be Q^N_α/N, and that of a doped O-rich hole to be $Q^{N+1}_\alpha - Q^N_\alpha$, then the average of these two compositions in the present case is 38.7% $d_{x^2-y^2}$, 50.2% p_σ, 6.9% a_z, 2.3% $d_{3z^2-r^2}$, and 2.0% p_π, which agrees fairly well with the values just mentioned aside from the modest $d_{x^2-y^2}$, p_σ imbalance.

IV. CONFIGURATION INTERACTION

It is the purpose of this section to carry out more accurate calculations of the quasiparticle energies in La_2CuO_4 than were obtained in the previous section using the HF approximation. Specifically, we are interested in the energies for adding $\epsilon^+_{\mathbf{k}}$ and removing $\epsilon^-_{\mathbf{k}}$ one hole of momentum $\mathbf{k}$ to the parent antiferromagnetic insulator. In principle, this requires calculation of the spectral weight, the imaginary part of the appropriate one-particle Green's function. There are, however, a number of calculations for the simpler but relevant t-J Hamiltonian which suggest that such spectral functions show quasiparticle peaks with large weights at the edge of the insulating gap for $\mathbf{k}$ vectors along the line between $\mathbf{k}_X$ and $\mathbf{k}_M$.[40–43] For these points, the quasiparticle energies then reduce to

$$\epsilon^+_{\mathbf{k}} = E^{N+1}_{\mathbf{k}} - E^N_0, \tag{17}$$

$$\epsilon^-_{\mathbf{k}} = E^N_0 - E^{N-1}_{\mathbf{k}}. \tag{18}$$

Here $E^n_{\mathbf{k}}$ is the lowest total energy for n holes with total momentum $\mathbf{k}$, there are N formula units in the system, and the ground state of the parent insulator ($n=N$) occurs for $\mathbf{k}$=0. In this section we improve our calculation of $E^n_{\mathbf{k}} = \langle\Psi^n_{\mathbf{k}} \mid H \mid \Psi^n_{\mathbf{k}}\rangle$ by representing $\Psi^n_{\mathbf{k}}$ in a limited configuration-interaction (CI) expansion beyond the HF approximation of the previous section.

While the HF approximation is trivially exact in the limit of vanishing two-body interactions, it omits important zero-point spin fluctuations from the ground states of Hubbard models when Coulomb interactions are finite. This deficiency is certainly evident in the case of the Néel solution for the $U \to \infty$ limit of the one-band model. Our limited CI procedure is a systematic attempt to restore some of these missing fluctuations, by diagonalizing the many-body Hamiltonian within a set of configurations which includes metastable HF solutions for alternate, low-energy spin arrangements in addition to the HF ground state. Since spin order in the cuprates is keyed to the $d_{x^2-y^2}$ orbitals, enumeration of these spin-fluctuation configurations is the same for both one-band and multiband models, i.e., depends only on the number of holes and not on the number of orbitals in the model. For this reason, we test our CI procedure for the one-band model, where comparison may be made to exact results, in addition to carrying out the desired calculations for the eight-band effective Hamiltonian. We take the standard form for the one-band Hubbard Hamiltonian,

$$H = -t\sum_{<i,j>,\sigma}(c^\dagger_{i\sigma}c_{j\sigma} + \text{H.c.}) + U\sum_i n_{i\uparrow}n_{i\downarrow}, \tag{19}$$

where $\langle i,j\rangle$ singly counts near-neighbor links and $n_{i\sigma} \equiv c^\dagger_{i\sigma}c_{i\sigma}$.

In the remainder of this section, we first describe the set of spin configurations used in our CI calculations, and the manner of their generation. As these configurations are nonorthogonal, evaluation of the many-body Hamiltonian and overlap matrix elements required for the CI eigenvalue problem is nontrivial, and is therefore briefly discussed. Finally, we present our limited CI results for the quasiparticle energies at $\mathbf{k}_X$ and $\mathbf{k}_M$ for both the one-band Hubbard model and the eight-band Hamiltonian in Eq. (2).

A. Spin configurations

We begin here with a discussion of spin configurations important to the intrinsic N-hole insulator, and then turn to the (N±1)-hole doped systems. In the first case, a specific example of the inadequacy of a mean-field solution in the Heisenberg limit of the one-band Hubbard is illuminating. The exact, singlet ground state of the periodic, four-site, antiferromagnetic Heisenberg model is a linear combination of six spin configurations,

$$\Psi_0 = \frac{1}{\sqrt{12}}(2\,|\uparrow\downarrow\uparrow\downarrow\rangle - |\uparrow\downarrow\downarrow\uparrow\rangle - |\downarrow\uparrow\uparrow\downarrow\rangle - |\uparrow\uparrow\downarrow\downarrow\rangle - |\downarrow\downarrow\uparrow\uparrow\rangle + 2\,|\downarrow\uparrow\downarrow\uparrow\rangle), \tag{20}$$

where $|\uparrow\downarrow\uparrow\downarrow\rangle \equiv c^\dagger_{1\uparrow}c^\dagger_{2\downarrow}c^\dagger_{3\uparrow}c^\dagger_{4\downarrow} \mid \text{vac}\rangle$, and sites 2 and 4 are near neighbors of site 1. The two Néel configurations, $|\uparrow\downarrow\uparrow\downarrow\rangle$ and $|\downarrow\uparrow\downarrow\uparrow\rangle$, are the degenerate ground states of the Heisenberg antiferromagnet in the mean-field approximation, and are analogous to HF ground states of the finite-U Hubbard model. The inner configurations in Eq. (20) are mean-field solutions which are O(J) higher in energy, and may be viewed as zero-point fluctuations about the rigid order of the Néel configurations. Our limited CI procedure seeks to supplement the mean-field HF solutions with finite-U analogues of such fluctuations.

While HF solutions at finite U are single Slater determinants of Bloch rather than localized orbitals as in Eq. (20), the underlying spin order associated with the localized $d_{x^2-y^2}$ orbitals is evident from the appropriate diagonal elements $\rho_\sigma(i\alpha, i\alpha)$ of the one-particle density matrix Eq. (12). In particular, the HF ground states for one-band and multiband Hubbard models of the cuprates are Néel ordered, although the polarization at each Cu site is, of course, not complete. Moreover, we find that

self-consistent, metastable N-hole HF solutions for other spin arrangements may be obtained simply by reflecting the desired order in the initial guess for the density matrix, e.g., $\rho_\sigma(i\alpha, i\alpha)=1$ for $\alpha=d_{x^2-y^2}$ and *one* of the spin choices, and 0 otherwise. There is relaxation of these values in the converged density matrix, however, the input spin order persists in the sign of the $d_{x^2-y^2}$ spin density at the various Cu sites. It is the metastability of such HF solutions which makes the present limited CI procedure possible.

There is a one-to-one correspondence between the metastable HF solutions characterized by specific $d_{x^2-y^2}$ spin order, and the spin degrees of freedom in the Heisenberg Hamiltonian. There are, in particular, $N![(N/2)!]^{-2}$ eigenstates of the z component of the total spin $M_S=0$. These configurations may be categorized according to the number of spins which have been flipped (SF) relative to the Néel order, as indicated in Fig. 6, where "Néel" (a), "SF2" [(b) and (c)], and "SF4" [(d)–(i)] configurations are illustrated. Here the open (filled) arrows indicate unchanged (flipped) spins relative to the Néel order, and the inner shaded $\sqrt{8}\times\sqrt{8}$ diamonds (encompassing 4×4 squares) give configurations for $N=8$ ($N=16$). Note that flipped spins take precedence on the periodic boundaries of the $N=8$ clusters. Only configurations unrelated by symmetry are sketched in Fig. 6, while the two numbers to the right of each label give the number of configurations for $N=8$ and 16, respectively, which are generated from these prototypes by the action of translation and/or C_{4v} point group operators. All 70 possible $M_S=0$ spin configurations for $N=8$ are accounted for by the two leftmost columns, Figs. 6(a), 6(b), 6(d), 6(e), 6(g), and 6(h). The configurations implied by Fig. 6

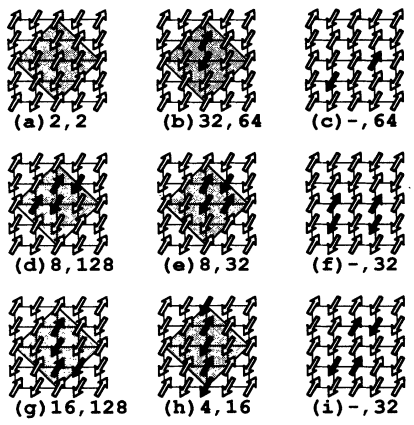

FIG. 6. Unique spin configurations for singly occupied sites of $N=8$ (shaded $\sqrt{8}\times\sqrt{8}$ diamonds) and $N=16$ (encompassing 4×4 squares) periodic clusters: (a) Néel, (b) and (c) SF2, and (d)–(i) SF4. Open (filled) arrows indicate unchanged (flipped) spins relative to the Néel order. Note that flipped spins take precedence on the periodic boundaries of the $N=8$ clusters. The numbers of symmetry-related configurations for $N=8$ and 16, respectively, are given below each diagram.

for $N=16$, however, account for only 4% of the corresponding 12 870 total (9 of the possible 123 symmetry-unrelated configurations). Nevertheless, these 498 configurations include those with the smallest number of energetically unfavorable ferromagnetic near-neighbor links, and are ones which we have found to be the most important in extensive numerical searches.

We turn now to $(N\pm1)$-hole configurations, and specifically only the $N+1$ case, since the electron-doped counterpart is quite similar. In principle, all $M_S=\frac{1}{2}$, $(N+1)$-hole spin configurations may be generated by adding an additional up-spin hole in all possible ways, to all possible $M_S=0$, N-hole spin configurations. In practice, we start with just those low-energy N-hole spin configurations implied by Fig. 6, and from each of these, construct 14 candidate $(N+1)$-hole configurations by selecting first the lowest-energy available orbital, then the second lowest, and so on, for the added $(N+1)$st hole. From this large set of candidate configurations, only those which had noticeable impact ($\sim 10^{-4}$ eV) on the total energy either at $\mathbf{k}_X$ or $\mathbf{k}_M$, when included in relatively small test CI calculations, were retained for further use.

We created all $(N+1)$-hole configurations by populating the various empty orbitals in the self-consistent N-hole HF solutions (rigid-band doping), *without* achieving further $(N+1)$-hole self-consistency. As noted in Sec. III C, $(N+1)$-hole self-consistency leads to $\mathbf{k}$-dependent variations in translational symmetry for the doped Néel configurations, i.e., those created by adding an $(N+1)$st hole to the Néel configuration in Fig. 6(a). We also found that some doped counterparts of the spin-flipped configurations in Fig. 6 were not metastable in self-consistent $(N+1)$-hole calculations. The use of configurations obtained by rigid-band doping therefore appeared to be the most systematic and reliable procedure for the $(N+1)$-hole CI calculations. Moreover, we did carry out several tests in which selected configurations, e.g., just the doped Néel or spin-bag (discussed below) configurations, were replaced by their $(N+1)$-hole self-consistent counterparts, and found little impact on the final CI total energies, or in some cases slightly higher total energies.

We believe the set of $(N+1)$-hole configurations just discussed to be relatively complete in regard to calculating the quasiparticle dispersion in La_2CuO_4, and it is precisely this set which was used in our previous work.[13,14] We suggest in this paper, however, that the "active ingredient" in the large number of doped spin-flipped configurations just discussed is the Bloch-projected spin bag of Sec. III C, at least insofar as the quasiparticle dispersion is concerned. We will demonstrate this fact by showing that the quasiparticle energies $\epsilon_{\mathbf{k}}^{+}=E_{\mathbf{k}}^{N+1}-E_0^N$ are already relatively well converged when just the doped Néel and spin-bag configurations are included in the CI calculations. The additional configurations appear to relax the rigid Néel approximation to the background spin system, reducing both $E_{\mathbf{k}}^{N+1}$ and E_0^N, yet leave the difference relatively unchanged. Conversely, omitting only the spin-bag configurations from the most complete set of CI configurations has a negligible effect on the resulting total energies.

B. Many-body matrix elements

Nonorthogonality between different spin configurations introduces a great deal of complexity into our limited CI calculations in addition to the required solution of the generalized eigenvalue problem. Specifically, evaluating expectations of the Hamiltonian operators between two configurations requires a numerical implementation of Wick's theorem[44] in the form of determinants. Given two HF states expressed in two different single-particle bases,

$$|\Psi\rangle = \prod_{\kappa\sigma} c^+_{\kappa\sigma}|\text{vac}\rangle, \tag{21}$$

$$|\Psi'\rangle = \prod_{\kappa'\sigma'} c^+_{\kappa'\sigma'}|\text{vac}\rangle, \tag{22}$$

the overlap is

$$\langle\Psi|\Psi'\rangle = \begin{vmatrix} \langle\kappa_1\sigma_1|\kappa'_1\sigma'_1\rangle & \langle\kappa_1\sigma_1|\kappa'_2\sigma'_2\rangle & \cdots \\ \langle\kappa_2\sigma_2|\kappa'_1\sigma'_1\rangle & \langle\kappa_2\sigma_2|\kappa'_2\sigma'_2\rangle & \\ \vdots & & \ddots \end{vmatrix}. \tag{23}$$

Similarly, the matrix element for a one-body operator is

$$\langle\Psi|c^+_\alpha c_\beta|\Psi'\rangle = -\begin{vmatrix} 0 & \langle\beta|\kappa'_1\sigma'_1\rangle & \langle\beta|\kappa'_2\sigma'_2\rangle & \cdots \\ \langle\kappa_1\sigma_1|\alpha\rangle & \langle\kappa_1\sigma_1|\kappa'_1\sigma'_1\rangle & \langle\kappa_1\sigma_1|\kappa'_2\sigma'_2\rangle & \cdots \\ \langle\kappa_2\sigma_2|\alpha\rangle & \langle\kappa_2\sigma_2|\kappa'_1\sigma'_1\rangle & \langle\kappa_2\sigma_2|\kappa'_2\sigma'_2\rangle & \\ \vdots & & & \ddots \end{vmatrix}, \tag{24}$$

and that for a two-body operator is

$$\langle\Psi|c^+_\alpha c^+_{\alpha'} c_{\beta'} c_\beta|\Psi'\rangle = \begin{vmatrix} 0 & 0 & \langle\beta|\kappa'_1\sigma'_1\rangle & \langle\beta|\kappa'_2\sigma'_2\rangle & \cdots \\ 0 & 0 & \langle\beta'|\kappa'_1\sigma'_1\rangle & \langle\beta'|\kappa'_2\sigma'_2\rangle & \cdots \\ \langle\kappa_1\sigma_1|\alpha\rangle & \langle\kappa_1\sigma_1|\alpha'\rangle & \langle\kappa_1\sigma_1|\kappa'_1\sigma'_1\rangle & \langle\kappa_1\sigma_1|\kappa'_2\sigma'_2\rangle & \cdots \\ \langle\kappa_2\sigma_2|\alpha\rangle & \langle\kappa_2\sigma_2|\alpha'\rangle & \langle\kappa_2\sigma_2|\kappa'_1\sigma'_1\rangle & \langle\kappa_2\sigma_2|\kappa'_2\sigma'_2\rangle & \\ \vdots & & & & \ddots \end{vmatrix}. \tag{25}$$

The leading zeros and signs result from commutations to get creation operators on the right. These equations follow simply from the idempotence of the antisymmetrization operator.

Determinant evaluation scales computationally as the size of the matrix cubed. Block diagonalizing into spin up and spin down is trivial and reduces the cost by a factor of $2^3 = 8$. Additional and significant reduction in the number of distinct many-body matrix elements which need to be calculated comes from acknowledging the relationships between spin configurations generated by the action of the translation and point-group operators on the unique N-hole configurations in Fig. 6, and similarly for their $(N+1)$-hole counterparts. That is, $\langle\Psi|g_1^{-1}Hg_2|\Psi'\rangle = \langle\Psi|Hg_3|\Psi'\rangle$, where g_1, g_2, and $g_3 = g_1^{-1}g_2$ are two-dimensional $p4mm$ space-group operators. In this regard, note that only the Néel configuration (a) in Fig. 6 has well-defined crystal momentum $\mathbf{k}$ relative to the antiferromagnetic double cell. However, nothing is gained by forming linear combinations of the spin configurations to obtain states with a particular momentum, since the above matrix elements must be evaluated on a determinant by determinant basis. Such restructuring of the many-body Hamiltonian and overlap matrices is feasible, but not warranted given the modest size (< 1000) of the matrices involved in this work. Rather, we solve the generalized eigenvalue problem in the complete space of all of the spin configurations discussed previously, effectively treating all momenta simultaneously. Having translation and point-group operators as generators for degenerate spin configurations greatly facilitates identification of the symmetry characteristics of these solutions, which we find to naturally exhibit well-defined $\mathbf{k}$ relative to the double-cell Brillouin zone.

C. Numerical results

We summarize here the numerical results from our limited CI calculations of the ground-state energy E_0^N for the N-hole insulator, and then the lowest energy $E_{\mathbf{k}}^{N+1}$ for the $(N+1)$-hole system of momentum $\mathbf{k}$, which together provide the addition energy $\epsilon_{\mathbf{k}}^+$ of Eq. (17). Values are given both for the one-band Hubbard model with $U/t = 16$, and for the eight-band Hamiltonian defined in Eq. (2). Finally, the $(N-1)$-hole case is discussed for the eight-band Hamiltonian and our results for the insulating gap in La_2CuO_4. All calculations were carried out for $\sqrt{8}\times\sqrt{8}$ ($N=8$) and 4×4 ($N=16$) formula-unit periodic clusters, although limited results are also given for

TABLE II. Ground-state energy per site E_0^N/N (in units of t) for the half-filled, one-band Hubbard model with $U/t = 16$. Results are given as a function of the number of sites N in the periodic clusters, and as a function of the CI expansion.

N	8	16	∞
Néel	−0.2390	−0.2445	−0.2453
+SF2	−0.2613	−0.2670	
+SF4	−0.2834	−0.2715	
Exact	−0.2845	−0.2882[a]	-0.288 ± 0.004[b]

[a]Reference 45.
[b]Estimated, see Ref. 46.

$\sqrt{32} \times \sqrt{32}$ ($N = 32$) clusters in the case of the eight-band Hamiltonian.

Table II gives our limited CI ground-state energies E_0^N for the half-filled, one-band Hubbard model. Recall that the Néel+SF2+SF4 configurations for the eight-site case exhaust the $M_S = 0$ manifold, and so the close agreement of the ground-state energy compared to the exact result for this N attests to the complete dominance of the spin fluctuations at $U/t = 16$. While our Néel+SF2+SF4 calculation for the 16-site case is seen to account for only 62% of the correlation energy, compared to the exact result,[45] it should be noted that it does so using only 4% of the configurations in the $M_S = 0$ manifold. We suggest that the 16-site case is already representative of the bulk, as indicated by the extrapolation of the exact value of E_0^N/N to the $N = \infty$ limit.[46]

Our corresponding results for the eight-band effective Hamiltonian are given in Table III. Considering that a one-band effective t for the cuprates is $\sim$0.5 eV,[5,6,9] the reductions in total energy brought about by adding the SF2 and then the SF4 spin configurations are comparable to those in Table II.

Table IV presents our limited CI calculations for the one-band Hubbard model with one hole added to the insulator. Only the X-point results are given, due to the degeneracy of the total energy at $\mathbf{k}_X$ and $\mathbf{k}_M$ for both the $\sqrt{8} \times \sqrt{8}$ and 4×4 implementations of this model.[47] Note also that the exact ground-state energy E_X^{N+1} corresponds to a total spin $S = \frac{3}{2}$, and not $\frac{1}{2}$, for the $N = 8$ case.[47] The "doped Néel" entries for E_X^{N+1} are expectations of H in the corresponding single configurations. The "spin-bag" entries here, and throughout this section, refer to the multiconfigurational projection states given by Eq. (15), which have well-characterized momentum. The entries labeled "both" refer to variationally optimized linear combinations of both the doped Néel configuration and the spin-bag state for the same momentum. That these values are essentially identical to the spin-bag entries attests to the redundancy of the doped Néel configurations in the case of the one-band Hubbard model, as mentioned in Sec. III C. The "+SF2" and "+SF4" labels refer to further augmentation of the limited CI by the $(N+1)$-hole counterparts of the SF2 and SF4 configurations in Fig. 6, as discussed earlier. The subtractions required to obtain the quasiparticle energies $\epsilon_X^+ = E_X^{N+1} - E_0^N$ were carried out using the corresponding entries in Tables II and IV, except that the "Néel" value of E_0^N in Table II was used in conjunction with each of the "doped Néel," "spin-bag," and "both" values for E_X^{N+1} in Table IV.

TABLE III. Ground-state energy per formula unit E_0^N/N (in eV) for the eight-band Hubbard Hamiltonian [Eq. (2)] as a function of the number of formula units N in the periodic clusters, and as a function of the CI expansion. These results are for the antiferromagnetic insulator with $n = N$ holes.

N	8	16	32
Néel	−2.0325	−2.0463	−2.0480
+SF2	−2.0400	−2.0625	
+SF4	−2.0504	−2.0669	

TABLE IV. Total energy E_X^{N+1} and quasiparticle energy $\epsilon_X^- = U - \epsilon_X^+$ (in units of t) for the one-band Hubbard model with $U/t = 16$, as a function of the number of sites N in the periodic clusters, and the CI expansion. The spin-bag entries refer to Bloch projections of the localized spin-bag configuration.

N	8	16
	E_X^{N+1}	
Doped Néel	13.867	11.851
Spin bag	12.670	10.473
Both	12.670	10.472
+SF2	12.275	9.966
+SF4	11.941	9.814
	$\epsilon_X^- = U - \epsilon_X^+$	
Doped Néel	0.221	0.238
Spin bag	1.418	1.615
Both	1.418	1.616
+SF2	1.635	1.762
+SF4	1.792	1.843
Exact	1.830	2.17[a]

[a]Estimated, see Ref. 48.

The numerical results for $\epsilon_X^- = U - \epsilon_X^+$ in Table IV serve to emphasize the importance of the spin-bag configurations to the nature of quasiparticles in the one-band Hubbard model. The multiconfigurational spin-bag state $|SB, \mathbf{k}_X\rangle$ accounts for over 70% of the difference between the doped Néel entries, which are just HF one-particle eigenvalues for the parent insulator due to Koopman's theorem, and the exact (or estimated[48] for $N = 16$) quasiparticle energies. Most (63% out of 71% for $N = 16$) of this improvement over the HF one-particle eigenvalues could be obtained from the single Slater determinant $|SB, \mathbf{R}\rangle$, and so has nothing to do with correlation, but rather with the very different nature of the states (including mean-field solutions) for this Hamiltonian with N versus $N+1$ particles. Inclusion of all of the SF2 and SF4 spin configurations in the CI calculation results in an excellent value of ϵ_X^- for $N = 8$, and one which has made up 83% of the difference between the starting doped Néel

value and the estimated exact result for $N=16$.

Table V gives our corresponding $(N+1)$-hole results for the eight-band Hamiltonian. It is immediately apparent that the doped Néel configurations are energetically competitive, and, in fact, the state at $\mathbf{k}_M$ is slightly lower in energy than the corresponding spin-bag state. It is also interesting to note that the doped Néel configurations and the spin-bag states predict different ordering of the quasiparticle energies $\epsilon_M^+ - \epsilon_X^+ = E_M^{N+1} - E_X^{N+1}$, with the two predictions differing by ~ 0.5 eV. The most important conclusion evident from Table V, however, is simply that both configurations are important. Moreover, the question of the $\mathbf{k}_M$-$\mathbf{k}_X$ dispersion appears to be settled already at the level of including both types of configurations, i.e., that the two points are nearly degenerate. Polarized spectroscopy measurements clearly require ϵ_X^+ to be lower, however, the data would not be inconsistent with $\epsilon_M^+ - \epsilon_X^+ \sim 0.1$ eV, which is within the uncertainties in our calculations. Note that ϵ_M^+–ϵ_X^+ and $\epsilon_X^+ = E_X^{N+1}$–E_0^N are already converged to within 0.02 and 0.06 eV, respectively, once both doped Néel and spin-bag configurations are included, even though the total energy E_X^{N+1} changes by 0.4 eV upon addition of the SF2 and SF4 spin fluctuations. This suggests that quantitative conclusions can be made about the quasiparticle energies without fully relaxing the rigid Néel order of the background.

Table VI gives some idea of how the nature of the wave functions used in Table V depend on the various CI expansions. A decomposition of the charge $\Delta n_{\mathbf{k}}(\alpha\sigma)$ associated with an added hole is presented,

$$\Delta n_{\mathbf{k}}(\alpha\sigma) = \sum_i \left(\langle \Psi_{\mathbf{k}}^{N+1} | n_{i\alpha\sigma} | \Psi_{\mathbf{k}}^{N+1} \rangle - \langle \Psi_0^N | n_{i\alpha\sigma} | \Psi_0^N \rangle \right), \tag{26}$$

where $M_S = \frac{1}{2}$ and 0 for $\Psi_{\mathbf{k}}^{N+1}$ and Ψ_0^N, respectively. Thus regardless of how the various configurations are generated, Eq. (26) examines the disposition of a net added up-spin hole to the parent insulator. The decomposition for the doped Néel case is just that of the one-particle HF orbital occupied by the $(N+1)$st hole, which shows 77% of the net added up-spin density going onto O sites and 23% onto Cu sites, with $\mathbf{k}$-dependent variations in the balance amongst the various O or Cu orbitals. These ratios are approximately reversed (~30% O and ~70% Cu) for the *added up-spin* density in the spin-bag case, however, an associated backflow of *preexisting down-spin* density from $d_{x^2-y^2}$ to the neighboring p_σ and a_z orbitals results in about the same change in *total* charge density as for the doped Néel case. Given these very different signatures, it is quite clear from the entries labeled "both" in the table, that the CI admixture of the doped Néel and spin-bag states is a true compromise, suggesting that both ingredients are important constituents of the optimal wave function. Moreover, on the scale of the differences between these two kinds of states, we judge that their simple admixture labeled "both" is in reasonable agreement with the more extensive CI results labeled "+SF2" and "+SF4," consistent with the behavior of the energy results in Table V.

The most prominent non-three-band component in Table VI is the ~30% a_z composition of an added hole at

TABLE V. Total energies $E_{\mathbf{k}}^{N+1}$ and quasiparticle dispersion $\epsilon_M^+ - \epsilon_X^+$ (in eV) for the eight-band Hubbard Hamiltonian [Eq. (2)] as a function of the number of formula units N in the periodic clusters, and as a function of the CI expansion. The spin-bag entries refer to Bloch projections of the localized spin-bag configuration.

N	8	16	32
	E_X^{N+1}		
Doped Néel	−15.068	−31.580	−64.379
Spin bag	−15.359	−31.976	−64.788
Both	−15.559	−32.104	−64.935
+SF2	−15.666	−32.420	
+SF4	−15.671	−32.497	
	E_M^{N+1}		
Doped Néel	−15.308	−31.810	−64.605
Spin bag	−15.098	−31.737	−64.538
Both	−15.536	−32.080	−64.883
+SF2	−15.619	−32.369	
+SF4	−15.619	−32.467	
	$\epsilon_M^+ - \epsilon_X^+$		
Doped Néel	−0.240	−0.230	−0.226
Spin bag	0.261	0.239	0.250
Both	0.023	0.024	0.052
+SF2	0.048	0.051	
+SF4	0.052	0.030	

TABLE VI. Decomposition (%) of the charge $\Delta n_{\mathbf{k}}(\alpha\sigma)$ associated with adding one ↑ hole of momentum $\mathbf{k}_X$ or $\mathbf{k}_M$ to the $N=16$ parent insulator, as a function of the CI expansion. Double-row entries indicate spin $\sigma = \uparrow, \downarrow$. Spin-bag entries are Bloch projections.

α	$d_{x^2-y^2}$	$d_{3z^2-r^2}$	p_σ	p_π	a_z
		X			
Doped Néel	22.7	0.0	62.5	14.8	0.0
	0.0	0.0	0.0	0.0	0.0
Spin bag	67.0	0.3	30.9	1.3	0.5
	−43.6	3.1	26.6	1.2	12.7
Both	51.9	0.2	43.1	4.6	0.2
	−30.5	1.8	20.7	0.7	7.3
+SF2	40.7	1.0	49.6	5.0	3.8
	−16.0	0.8	11.7	0.3	3.1
+SF4	39.1	1.2	49.9	4.8	4.9
	−14.3	0.7	10.5	0.3	2.7
		M			
Doped Néel	8.4	13.7	25.4	0.0	52.5
	0.0	0.0	0.0	0.0	0.0
Spin bag	70.3	1.4	25.1	0.5	2.7
	−43.0	3.4	24.5	1.2	13.9
Both	35.4	7.9	29.4	0.2	27.1
	−20.8	1.2	14.1	0.5	5.0
+SF2	27.9	8.1	34.2	0.5	29.2
	−11.1	0.6	8.1	0.2	2.2
+SF4	28.3	7.5	36.8	0.7	26.7
	−10.4	0.6	7.6	0.2	2.0

TABLE VII. Total energy E_M^{N-1} and insulating gap $E_g = \epsilon_X^+ - \epsilon_M^-$ (in eV) for the eight-band Hubbard Hamiltonian [Eq. (2)] as a function of the number of formula units N in the periodic clusters, and as a function of the CI expansion. The spin-bag entries are Bloch projections.

N	8	16	32
	E_M^{N-1}		
Doped Néel	−14.914	−31.434	−64.232
Spin bag	−15.185	−31.854	−64.634
Both	−15.185	−31.858	−64.634
+SF2	−15.257	−32.072	
+SF4	−15.266	−32.143	
	$E_g = \epsilon_X^+ - \epsilon_M^-$		
Doped Néel	2.538	2.466	2.461
Spin bag	1.976	1.650	1.650
Both	1.776	1.518	1.503
+SF2	1.717	1.508	
+SF4	1.870	1.500	

$\mathbf{k}_M$, which remains fairly constant throughout the last three entries in the table. The dominant up-spin character of this a_z component indicates its doped Néel origin. We have furthermore verified that it is this orbital component in this configuration which is responsible for the shallow dispersion seen in Table V. Put another way, any calculation which omits *either* a_z orbitals *or* doped Néel configurations is likely to obtain a dispersion $\epsilon_M^+ - \epsilon_X^+$ which is too large by about 0.2 eV.

Finally, Table VII presents our limited CI results for the eight-band Hamiltonian in the case of one hole removed from the parent insulator, and, in particular, E_M^{N-1} for the M point, which we find to be the $(N-1)$-hole ground state both at the HF level as well as in our CI calculations. Since all of the $N-1$ holes here are of the same mostly Cu $d_{x^2-y^2}$ character, one might expect pronounced one-band character, which is consistent with the irrelevancy of the doped Néel configuration evident in the E_M^{N-1} values in Table VII. The doped Néel configurations do impact E_X^{N+1}, and therefore our calculated insulating gap, $E_g = \epsilon_X^+ - \epsilon_M^-$. However, it is clear from the table that inclusion of just the doped Néel and spin-bag configurations is sufficient to give a calculated gap accurate to within about 5%. Our most converged value is 1.5 eV, which may be compared to measured values in the range 1.8–2.0 eV.[36] This theoretical value includes a $\sim$ 1-eV reduction from the original HF M-to-X gap of about 2.5 eV in Fig. 2, which is consistent with solutions for one-band analogues for the cuprates. Specifically, for $U/t = 8$, we find the difference between the doped Néel gap E_g and that from exact 10-site calculations[47] to be $\sim 2t$, or about 1 eV for an effective one-band $t \sim 0.5$ eV.[5]

V. CONCLUSIONS

We give here our conclusions about the nature and dispersion of quasiparticle states associated with the addition of one hole or electron to insulating La_2CuO_4, as well as the impact of various levels of theoretical approximation on these properties.

(1) *Spin bags:* At the simplest theoretical level, our results suggest that Hartree-Fock (HF) theory alone can provide a surprisingly realistic description of the cuprate electronic structure, when the periodic Néel solution is taken for the parent N-hole insulator, and spatially inhomogeneous spin-bag solutions[21–30] are taken for the $(N \pm 1)$-hole doped materials. The corresponding total-energy differences are of approximately the correct size for the ionization and affinity quasiparticle energies, and the one-particle state densities exhibit an approximation to the doping-induced transfer of spectral weight that is characteristic of the cuprates.[1–5] A simple extension, Bloch projection of the localized spin-bag configurations to make multiconfigurational states of well-characterized momentum, also provides a first approximation to the dispersion: a 1.6-eV bandwidth for the doped holes, a lowest point at $\mathbf{k}_X = (\pi/2, \pi/2)$ populated by the first doped holes, and the $\mathbf{k}_M = (\pi, 0)$ point about 0.24 eV higher in hole energy.

(2) *Doped Néel configurations:* Our limited configuration-interaction (CI) results clearly point to the importance of a second class of $(N+1)$-hole configurations in the case of multiband cuprate models. These doped Néel configurations preserve the Néel order of the HF approximation to the insulating parent, in contrast to the spin-bag HF solutions which localize the doped, mostly O hole about a flipped Cu spin relative to the Néel-ordered parent. The doped Néel configurations may therefore provide the spin-flipped counterparts of the spin-bag configurations, which would be required to complete any local singlet relationship between the doped-O and intrinsic-Cu holes.[32] Our results suggest that the simple combination of spin-bag and doped Néel configurations given by Eq. (1) is sufficient to yield the dispersion $\epsilon_M^+ - \epsilon_X^+ = E_M^{N+1} - E_X^{N+1}$, the quasiparticle energy $\epsilon_X^+ = E_X^{N+1} - E_0^N$, and the total energy E_X^{N+1} converged to within about 0.02, 0.06, and 0.4 eV, respectively, for $N = 16$. These numbers imply significant cancellation between total energies in the first two quantities, which we attribute to inadequacies of the HF approximated spin background which do *not* impact the quasiparticle energies themselves. In this regard, our results are entirely consistent with other indications that the quasiparticle states are very localized excitations in the cuprates.[43] It should be emphasized that the importance of the doped Néel configurations depends crucially on the asymmetry in nature (O versus Cu) between doped and intrinsic particles, and that while they may be numerically generated, we find such configurations to be irrelevant for the one-band Hubbard model and for electron-doped or $(N-1)$-hole multiband models.

(3) *Dispersion:* Apical-O p_z components coming from doped Néel configurations are primarily responsible for reducing the above-mentioned $\epsilon_M^+ - \epsilon_X^+ = 0.24$-eV dispersion calculated solely with Bloch-projected spin-bag states to $\sim$0.04 eV in our most extensive CI calculations. The principal uncertainty in this value probably arises from the parameters in Table I,[49] rather than from the CI convergence (only about ± 0.02 eV). Polarized spectroscopy measurements[12,34] require $\epsilon_M^+ > \epsilon_X^+$, and we be-

lieve $\epsilon_M^+ - \epsilon_X^+ \sim 0.1$ eV is likely, given the consistency of this value with normal-state transport properties.[50] The essential point we wish to emphasize is that calculations which omit *either* a_z (apical-O p_z) components *or* doped Néel configurations are likely to obtain a value of $\epsilon_M^+ - \epsilon_X^+$ which is too large by ~ 0.2 eV. On the scale of the small inverse mass in the X to M direction, this is not a negligible error.

(4) *Composition:* Our most converged CI calculations suggest that the average Wannier function composition of the intrinsic holes in insulating La_2CuO_4 is a rather pristine $d_{x^2-y^2}$, p_σ mixture (64.7% $d_{x^2-y^2}$, 34.0% p_σ, 0.6% a_z, 0.3% $d_{3z^2-r^2}$, and 0.3% p_π), in contrast to the first hole doped into the insulator at $\mathbf{k}_X = (\pi/2, \pi/2)$ which we find to have ~15% non-three-band character (60.4% p_σ, 24.8% $d_{x^2-y^2}$, 7.6% a_z, 5.1% p_π, and 1.9% $d_{3z^2-r^2}$). Due to transfer of spectral weight, the doping-induced prepeak in O K-edge absorption spectra is a mixture of intrinsic and doped-hole characteristics.[2,3] A simple average of the the two compositions just mentioned (see also Sec. III D) suggests a p_z to $p_{x,y}$ polarization ratio of ~8%, which is the same order of magnitude as the 14% value obtained in recent experiments.[12] As for the intrinsic holes alone, we find a small $d_{3z^2-r^2}$ to $d_{x^2-y^2}$ ratio, 0.5%, which may be compared to the 1.5% value of Chen *et al.*,[12] however, we see no evidence for any significant z-polarized O($2p$) component in the perfect insulator.

VI. SUMMARY

We have reported limited configuration-interaction calculations beyond Hartree-Fock (HF) for an *ab initio* derived eight-band effective Hamiltonian describing La_2CuO_4. We find that quasiparticle states associated with the addition of one hole to the parent insulator may be well represented by a combination of two simple types of configurations which is suggestive of the Zhang-Rice singlet.[32] These spin-bag and doped Néel configurations may be easily generated by HF calculations, and the whole procedure carried out for effective Hamiltonians large enough to be chemically realistic, as in the present case. We have used this approach to establish numerically the crucial impact of apical-O p_z states on the quasiparticle dispersion in the important high-mass $(1,-1)$ direction away from the point $\mathbf{k} = (\pi/2, \pi/2)$ where the first holes are doped into the insulator.

ACKNOWLEDGMENTS

This work was financially supported by the U.S. Department of Energy under Contract No. W-7405-Eng-48. We gratefully acknowledge conversations with R. M. Martin as well as with C. T. Chen, J. E. Gubernatis, H. Q. Lin, S. Massidda, M. Posternak, G. A. Sawatzky, and S. A. Trugman.

[1] H. Romberg, M. Alexander, N. Nücker, P. Adelmann, and J. Fink, Phys. Rev. B **42**, 8768 (1990).
[2] C. T. Chen, F. Sette, Y. Ma, M. S. Hybertsen, E. B. Stechel, W. M. C. Foulkes, M. Schlüter, S.-W. Cheong, A. S. Cooper, L. W. Rupp, Jr., B. Batlogg, Y. L. Soo, Z. H. Ming, A. Krol, and Y. H. Kao, Phys. Rev. Lett. **66**, 104 (1991).
[3] H. Eskes, M. B. J. Meinders, and G. A. Sawatzky, Phys. Rev. Lett. **67**, 1035 (1991).
[4] E. Dagotto, A. Moreo, F. Ortolani, J. Riera, and D. J. Scalapino, Phys. Rev. Lett. **67**, 1918 (1991).
[5] S. B. Bacci, E. R. Gagliano, and R. M. Martin, in *Electronic Structure and Mechanisms of High Temperature Superconductivity*, edited by J. Ashkenazi and G. Vezzoli (Plenum, New York, in press).
[6] M. Hybertsen, E. Stechel, M. Schlüter, and D. Jennison, Phys. Rev. B **41**, 11 068 (1990).
[7] J. F. Annett and R. M. Martin, Phys. Rev. B **42**, 3929 (1990).
[8] S. B. Bacci, E. R. Gagliano, R. M. Martin, and J. F. Annett, Phys. Rev. B **44**, 7504 (1991).
[9] H. Eskes and G. A. Sawatzky, Phys. Rev. B **44**, 9656 (1991).
[10] A. Bianconi, P. Castrucci, A. Fabrizi, M. Pompa, A. M. Flank, P. Lagarde, H. Katayama-Yoshida, and G. Calestani, Physica C **162-164**, 209 (1989).
[11] H. Romberg, N. Nücker, M. Alexander, J. Fink, D. Hahn, T. Zetterer, H. H. Otto, and K. F. Renk, Phys. Rev. B **41**, 2609 (1990).
[12] C. T. Chen, L. H. Tjeng, J. Kwo, H. L. Kao, P. Rudolf, F. Sette, and R. M. Fleming, Phys. Rev. Lett. **68**, 2543 (1992).
[13] J. B. Grant and A. K. McMahan, Phys. Rev. Lett. **66**, 488 (1991).
[14] J. B. Grant, Ph.D. thesis, 1992.
[15] C. Di Castro, L. F. Feiner, and M. Grilli, Phys. Rev. Lett. **66**, 3209 (1991).
[16] V. I. Anisimov, M. A. Korotin, J. Zaanen, and O. K. Andersen, Phys. Rev. Lett. **68**, 345 (1992).
[17] A. K. McMahan, R. M. Martin, and S. Satpathy, Phys. Rev. B **38**, 6650 (1988).
[18] O. Gunnarsson, O. K. Andersen, O. Jepsen, and J. Zaanen, Phys. Rev. B **39**, 1708 (1989).
[19] M. S. Hybertsen, M. Schlüter, and N. E. Christensen, Phys. Rev. B **39**, 9028 (1989).
[20] A. K. McMahan, J. F. Annett, and R. M. Martin, Phys. Rev. B **42**, 6268 (1990).
[21] J. R. Schrieffer, X.-G. Wen, and S.-C. Zhang, Phys. Rev. Lett. **60**, 944 (1988); Phys. Rev. B **39**, 11 663 (1989).
[22] W. P. Su, Phys. Rev. B **37**, 9904 (1988).
[23] H.-Y. Choi and E. J. Mele, Phys. Rev. B **38**, 4540 (1988).
[24] A. Singh and Z. Tešanović, Phys. Rev. B **41**, 614 (1990).
[25] H. J. Schulz, Phys. Rev. Lett. **64**, 1445 (1990).
[26] K. Yonemitsu, I. Batistić, and A. R. Bishop, Phys. Rev. B **44**, 2652 (1991).
[27] M. Inui and P. B. Littlewood, Phys. Rev. B **44**, 4415 (1991).
[28] J. Zaanen and O. Gunnarsson, Phys. Rev. B **40**, 7391 (1989).
[29] K. Yonemitsu and A. R. Bishop, Phys. Rev. B **45**, 5530 (1992).
[30] K. Yonemitsu, A. R. Bishop, and J. Lorenzana (unpublished).
[31] We take the word "configuration" to be synonymous with "single Slater determinant" throughout the present paper.
[32] F. C. Zhang and T. M. Rice, Phys. Rev. B **37**, 3759 (1988).
[33] S. C. Miller and W. F. Love, *Tables of Irreducible Repre-*

sentations of Space Groups and Co-Representations of Magnetic Space Groups (Pruett, Boulder, 1967).

[34]F. J. Himpsel, G. V. Chandrashekhar, A. B. McLean, and M. W. Shafer, Phys. Rev. B **38**, 11946 (1988); H. Nücker, H. Romberg, X. X. Xi, J. Fink, B. Gegenheimer, and Z. X. Zhao, *ibid.* **39**, 6619 (1989).

[35]H. Eskes and G. A. Sawatzky, Phys. Rev. Lett. **61**, 1415 (1988); A. Fujimori, Phys. Rev. B **39**, 793 (1989); J. F. Annett, R. M. Martin, A. K. McMahan, and S. Satpathy, *ibid.* **40**, 2620 (1989); J. B. Grant and A. K. McMahan, Physica C **162-164**, 1439 (1989).

[36]S. L. Cooper, G. A. Thomas, A. J. Millis, P. E. Sulewski, J. Orenstein, D. H. Rapkine, S-W. Cheong, and P. L. Trevor, Phys. Rev. B **42**, 10785 (1990); T. Thio, R. J. Birgeneau, A. Cassanho, and M. A. Kastner, *ibid.* **42**, 10800 (1990).

[37]S. Massidda, M. Posternak, and A. Baldereschi (unpublished).

[38]S. Doniach and E. H. Sondheimer, *Green's Functions for Solid State Physicists* (Benjamin, Reading, 1974), p. 124.

[39]V. I. Anisimov, J. Zaanen, and O. K. Andersen, Phys. Rev. B **44**, 943 (1991).

[40]S. A. Trugman, Phys. Rev. B **41**, 892 (1990).

[41]K. J. von Szczepanski, P. Horsch, W. Stephan, and M. Ziegler, Phys. Rev. B **41**, 2017 (1990).

[42]E. Dagotto, A. Moreo, R. Joynt, S. Bacci, and E. Gagliano, Phys. Rev. B **41**, 2585 (1990).

[43]J. Song and J. F. Annett, Europhys. Lett. **18**, 549 (1992).

[44]W. Jones and N. H. March, *Theoretical Solid State Physics* (Wiley, London, 1973), Vol. 1, p. 560.

[45]H. Q. Lin, Phys. Rev. B **44**, 7151 (1991).

[46]We have estimated the $N=\infty$ ground-state energy E_0^N of the one-band Hubbard model at $U/t=16$ by comparing $E_0^N/(NJ)$ ($J=4t^2/U$ for the Hubbard model) as a function of $0 \le t/U \le 0.25$ for $N=8,10$ (Ref. 47) and $N=16$ (Ref. 45), including the Heisenberg limit $t/U=0$ [S. Nakagawa, T. Hamada, J. Kane, and Y. Natsume, J. Phys. Soc. Jpn. **59**, 1131 (1990)]. For both $t/U=0$ [N. Trivedi and D. M. Ceperley, Phys. Rev. B **41**, 4552 (1990)] and $t/U=0.25$ [S. R. While, D. J. Scalapino, R. L. Sugar, E. Y. Loh, J. E. Gubernatis, and R. T. Scalettar, Phys. Rev. B **40**, 506 (1989)] the $N=\infty$ limit is known. Taken together, these results suggest but do not prove that $E_0^N/(NJ)$ is already relatively well converged for $t/U > \frac{1}{16}$ by $N=16$, with $E_0^\infty/(NJ)$ likely to be within about 3% of $E_0^{16}/(NJ)$. Moreover, the curves cross near $t/U=\frac{1}{16}$, yielding weaker N dependence in this vicinity, so that we estimate $E_0^\infty/(NJ)=-1.15\pm0.015$ or $E_0^\infty/(Nt)=-0.288\pm0.004$ at $t/U=\frac{1}{16}$.

[47]E. Dagotto, R. Joynt, A. Moreo, S. Bacci, and E. Gagliano, Phys. Rev. B **41**, 9049 (1990).

[48]We have estimated the quasiparticle energy $\epsilon_X^- = 2.17t$ for the 16-site one-band Hubbard model at $U/t=16$ by interpolating available 10-site results [$\mathbf{k}=(3\pi/5,\pi/5)$, Ref. 47] to this value of U/t, and then using the appropriate 10- to 16-site difference for the t-J model [Y. Hasegawa and D. Poilblanc, Phys. Rev. B **40**, 9035 (1989)] to make the correction to 16 sites.

[49]We have carried out six-band limited CI calculations with the one-body parameters of Table I replaced by the values used in Fig. 1(b) of Ref. 15; however, we obtain $\epsilon_M^+ < \epsilon_X^+$ (by $\sim$0.25 eV), which conflicts with the implications of the polarized spectroscopy measurements of Refs. 12 and 34.

[50]S. A. Trugman, Phys. Rev. Lett. **65**, 500 (1900).

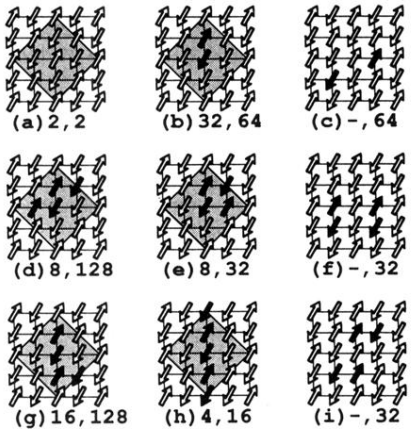

FIG. 6. Unique spin configurations for singly occupied sites of $N = 8$ (shaded $\sqrt{8} \times \sqrt{8}$ diamonds) and $N = 16$ (encompassing 4×4 squares) periodic clusters: (a) Néel, (b) and (c) SF2, and (d)–(i) SF4. Open (filled) arrows indicate unchanged (flipped) spins relative to the Néel order. Note that flipped spins take precedence on the periodic boundaries of the $N = 8$ clusters. The numbers of symmetry-related configurations for $N = 8$ and 16, respectively, are given below each diagram.